Towards DAS ship detection using signal-based features

P. Anhaus[a], A. Bueno Rodriguez[a], J. Schmidt[a], M. Stephan[a], and E. Peters[a]

[a]German Aerospace Center (DLR e. V.), Institute for the Protection of Maritime Infrastructures, Bremerhaven, Germany

ABSTRACT

Within the last decade, technological advancement and research development have enabled to exploit existing underwater fiber-optic cables for monitoring their environment as well as their intrinsic properties. Those cables are critical parts of the maritime infrastructure and are thus targets for sabotage through vessels and anchor drops. Vice versa, fiber-optic cables can be used to detect ships for, e.g., monitoring sea traffic in that area or maritime surveillance. Passing vessels perturb the water column and generate waves with distinct signatures at specific frequencies that can be sensed by the cables. In this study, we tested a set of statistical and signal-based features to detect ships using the distributed acoustic sensing (DAS) method. We analyzed the acoustic signature of a ship passing a telecommunication cable off the coast of Oregon. Our results showed that the selected features, energy envelope, spectral entropy, and frequency index, can detect ships, without considering additional environmental data. Thus, this study provides a compliment to existing studies for further automatic ship detection and with that the ability to protect the cable infrastructures.

Keywords: Distributed Acoustic Sensing (DAS), underwater telecommunication cables, ship acoustic signatures, protection of maritime infrastructures

1. INTRODUCTION

Critical maritime infrastructures, for example pipelines, submarine telecommunication and power cables, offshore wind parks, ports and ship routes require monitoring and protection from destruction by accidents and security. In the last three decades, the Distributed Acoustic Sensing (DAS) measurement technology has been shown to transform a standard fiber-optic cable into a dense array of thousands of individual vibration sensors. Natural sources such as wind, ocean and seismic waves, and biology as well as anthropogenic sources such as ships in the ocean emit acoustic signals that are sensed by those cables in form of vibrations at the cable itself.[1] By analyzing the acoustics signals sensed by the cables, events in the vicinity of submarine cables can be classified, which helps to protect the cables itself. On the other hand, by exploiting this technology, the submarine cables can in turn be used as perimeter control when spanned around maritime critical infrastructures. It has been shown that ships and boats,[2–7] aircrafts,[8] trains,[9] whales,[6,10] fish and crustaceans,[4] storms,[11] earthquakes,[11–15] ocean surface waves,[16] as well as the formation process of sea ice[17] emit acoustic signals at different frequencies with different acoustic energy. Those signals can be measured by DAS interrogators connected to fiber-optic cables.

The mechanical components of ships such as propellors, cavitation around the propellor blades, main and auxiliary engines, pumps, compressors, and generators and their interaction with the water column produce acoustic energy emitted into the ocean at specific frequencies. Zak (2008)[2] measured the level of vibration using accelerometers installed on machinery for five Polish Navy ships with lengths and widths ranging from 40 to 60 m and 7 to 8 m, respectively. They found relevant frequencies emitted by the different parts of 8 Hz for the shaft of the propeller, 30 Hz for the diesel generator, 40 Hz for the propeller blades, 50 Hz and 60 Hz for the main engines, and 150 Hz for the propeller. Those frequencies

Further author information: Send correspondence to Philipp Anhaus: E-mail: philipp.anhaus@dlr.de

Emerging Technologies and Materials for Security and Defence 2025, edited by Chantal Andraud, Roberto Zamboni, Andrea Camposeo, Luana Persano, Martin Laurenzis, Gerald S. Buller, Robert A. Lamb, Proc. of SPIE Vol. 13678, 136780P · 2025 Published by SPIE · 0277-786X · doi: 10.1117/12.3069711

were found in the underwater noise spectrum of the moving ships recorded by hydrophones. Niu et al. (2017)[3] showed that the shipping noise of three different cargo ships traveling at different speeds in the Santa Barbara Channel (CA, USA) measured by hydrophones is strongest between 30 Hz and 100 Hz. Reis et al. (2019)[4] computed signatures from underwater audio recordings to detect boats in preservation areas. They found several characteristic frequency peaks from 35 Hz up to 400 Hz. Rivet et al. (2021)[5] found the maximum energy received from a passing ship at a frequency of 49 Hz, as detected by a cable offshore of Toulon (France) using DAS. Ugalde et al. (2022)[18] presented the rotation speeds of the diesel generator of a ship passing a submarine cable close to the Canary Islands with 720 rpm which caused energy emitted between 6 Hz and 24 Hz with a peak at 6 Hz. They found those signatures in the power spectral density and spectrograms using DAS. Wilcock et al. (2023)[6] used DAS data from an underwater cable off the coast of Central Oregon (OR, USA) to identify the frequencies of acoustic energy emitted by a passing cargo ship. Using a spectrogram, the found energy between 10 Hz and 60 Hz. Paap et al. (2025)[19] calculated the power spectral density from DAS data recorded on two underwater cables, off the coast of Central Oregon and in the Dutch North Sea. They found vessel-related energy at frequencies above 50 Hz but below 100 Hz.

Within those studies, the acoustic characteristics of ships and their energy content were investigated using strain recordings, Fourier transforms, spectrograms, frequency-wavenumber power spectrum, and power spectra density. However, there are several more potential tools and parameters in signal processing to be tested to detect ships and their emitted energy. In this study, we used open access DAS data from an underwater cable off the coast of Central Oregon (OR, USA) to explore the performance of the energy envelope, the spectral entropy, and the frequency index to detect a passing ship. Those parameters provide an interesting complementary information on the detection of ships using DAS.

2. MEASUREMENT PRINCIPLE, DATA, AND STUDY SITE

A DAS interrogator measures the optical phase delay of the backscattered light to demodulate fluctuations in strain events along a fiber. The interrogator sends pulses of laser light at a wavelength of 1550 nm down a fiber. As the light travels, tiny natural imperfections in the glass scatter a small amount of the light back towards the interrogator. If the fiber experiences mechanical tension or compression at any point, e.g. through the pressure wave that ships emit, it will change the phase of the light that is backscattered from that point.[1,20,21]

We used DAS datasets as collected at a pre-installed telecommunication fiber-optic cable off the coast of Central Oregon (OR, USA) available through Wilcock et al. (2023)[6] and Wilcock & OOI (2023).[22] The cable was connected to a LUNA Optasense QuantX DAS interrogator that recorded the phase change at an original frequency of 1000 Hz, down-sampled to 500 Hz (0.002 s), with a spatial resolution (gauge length) of 30.6 m and a spatial sampling interval (channel spacing) of 2.04 m. In this study, we used #30 30 s-long datasets that were recorded between 01:51:01 UTC and 02:06:01 UTC on 3 November 2021 spanning 15 min of data.

The coastal area of Oregon is characterized by high ship traffic with ships traveling on south-north routes as well as on transpacific routes with, e.g., 5 to 25 million containers being shipped in 2018.[23]

3. SIGNAL ANALYSIS

We used strain data, spectrograms, energy envelopes, spectral entropy, and frequency index to investigate the performance of those parameters in detecting the ship. The signal analysis is based on two opposing cases when no ship was present and when the ship was present.

3.1 Strain

Strain induced at a fiber segment due to a pressure wave leads to a change in the mechanical lengths and in the refractive index of glass through the photo-elastic effect.[20] We followed Wilcock & OOI (2023)[22] and the SEAFOM Fiber Optic Monitoring Group[20] to convert the phase into strain. This included removing the mean phase from the timeseries to unwrap the phase, converting into units of radians, and applying a photo-elastic scaling factor for fused silica. As a result, the phase change is proportional to the strain and a constant. We applied a band-pass filter to the strain data with cutoff frequencies at the lower end of 5 Hz and at the upper end of 100 Hz following Paap et al. (2025).[19]
The strain data shows a ship that passed the telecommunication cable at a distance from the coast (0 m) of approximately 46 900 m to 50 370 m between 01:51:31 UTC and 02:05:01 UTC on 3 November 2021 (e.g., Figure 1,[6,19,22]). The water depth at the ship's passing was between 400 m and 500 m.[6] We identified the ship as the cargo ship *Elsa Oldendorff* (IMO 9702625, MMSI 255613000, length 180 m, width 30 m) using an AIS toolbox that implements AIS data from AISHub (https://www.aishub.net).[24]

We selected two cases, when no ship was present (Figure 1a, start time 01:51:01 UTC) and when the

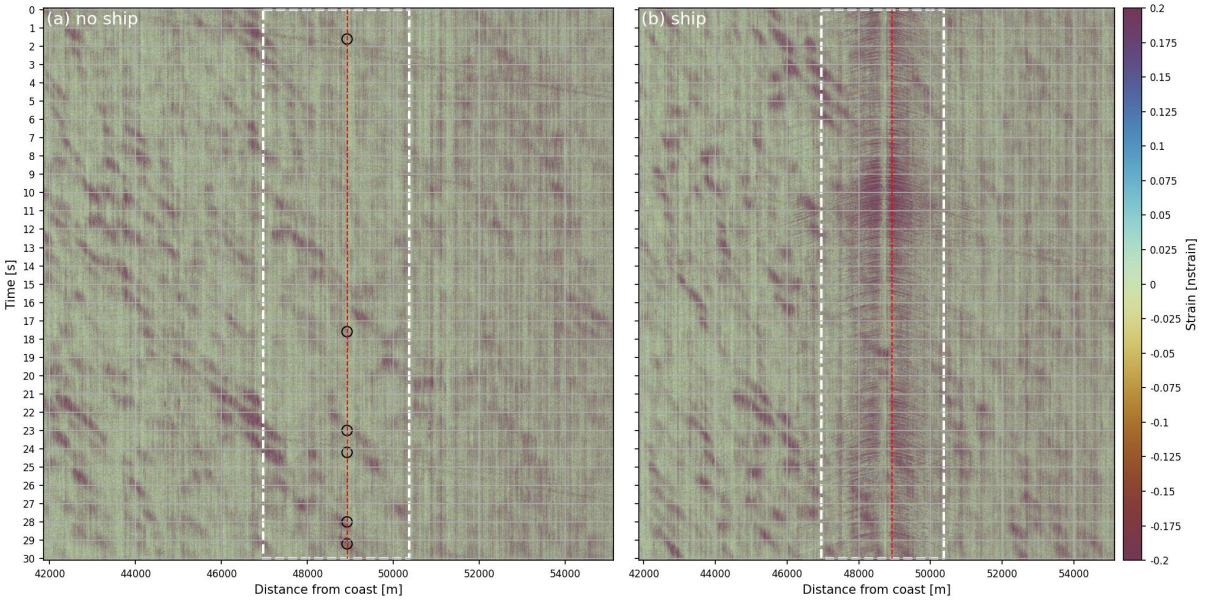

Figure 1: 30 s strain data as recorded off the coast of Central Oregon (OR, USA) on 3 November 2021. (a) Start time 01:51:01 UTC, no ship and (b) start time 01:58:01 UTC, ship is present. The origin of the fiber position (0 km) is relative to the shoreline. The white, dashed rectangles highlight the areas that we have selected for further analysis. Number of channels were # 1 670 from 23 000 to 24 670. The red, dashed lines indicate the individual channel # 23 960. The black circles in (a) indicate relevant positions for the spectrogram analysis below.

ship was present (Figure 1b, start time 01:58:01 UTC). At 01:51:01 UTC (Figure 1a), the ship was not yet detected by the fiber-optic cable. 30 s later, at 01:51:31 UTC, the ship was detected for the first time (not shown). At 01:58:01 UTC, the acoustic signature of the ship was clearly detected (Figure 1b). The highest strain was spatially confined to approximately 3 410 m (#1 670 channels) between 46 964 m and 50 374 m, besides a small gap within the center of the triangular shape where the strain was close to zero. Shortly after 02:04:35 UTC, the signature was not visible in the strain recordings anymore (not shown).

3.2 Spectrogram

Here, we investigate spectrograms that visually represent the frequency content of the strain signals over time. We computed the short-time Fourier transform (STFT) of the strain for the #1 670 channels. Then, we computed the spectrograms from the absolute of each of the STFTs for the #30 30 s datasets. This resulted in one value for each timestep of 0.002 s along each channel.

Figure 2a shows the spectrogram for the entire 900 s (15 min) timeseries of the strain between 01:51:31 UTC and 02:05:01 UTC. The spectrogram reveals elevated energy at frequencies between 40 Hz and 65 Hz during 300 s (5 min) and 750 s (12 min), between 01:56:01 UTC and 02:03:01 UTC. The spectrogram shows an alternating pattern with increasing and decreasing energy and elevated energy occurring every 27 s. The maxima of the energy were recorded between 390 s and 420 s and between 420 s and 450 s referring to the 30 s windows starting at 01:57:31 UTC and 01:58:01 UTC (Figure 1b), respectively.

Along the entire timeseries, the spectrogram shows another band of elevated energy at frequencies between 5 Hz and 20 Hz. This band of elevated energy was strongest when the energy at frequencies between 40 Hz and 65 Hz was elevated, between 300 s and 750 s.

Panels (b) and (c) show zoom-in spectrograms for the 420 to 450 s (b, ship case, 01:58:01 UTC) and 0 to 30 s (c, no-ship case, 01:51:01 UTC) periods, respectively. Elevated energy between 40 Hz and 65 Hz was present throughout the entire 30 s window (b). The energy content peaked between 429 s and 432 s and lasted for approximately 3 s. The band of elevated energy at frequencies between 5 Hz and 20 Hz was also present throughout. In the spectrogram of the no-ship case (c), a band of elevated energy was more confined in frequency centered at 10 Hz. There were several peaks of elevated energy that stretched across the entire frequency range, e.g., at 24 s and 27 s.

We selected the individual cable channel #23 960 at which the ship's signal was clearly detected (red, dashed line in Figure 1b) and compared the results to the same channel for the dataset when the ship was not present (Figure 1a). For the spectrograms of the individual channel #23 960 (Figure 2d, e), we converted the amplitude spectrograms to dB-scaled spectrograms by taking the squared absolute of the amplitude spectrograms and referencing it to its squared maximum value. We also normalized those spectrograms by the mean spectrogram of the ship case.

The spectrogram for the ship case (d) also shows a high amplitude of 0 db at frequencies between 40 Hz and 65 Hz for the time period 429-432 s. This signal is visible also as a band for almost the entire recorded time period of 30 s but with weaker amplitudes. Signals at other frequencies were not significant. When the ship was not present (e), the spectrogram shows scattered peaks of elevated amplitudes at frequencies centered at 10 Hz. Those peaks occurred between 1.5-1.7 s, between 17-18 s, at 23 s, at 28 s, and between 29-29.5 s (black circles). We conclude that those peaks are not associated with the ship. The peaks are rather associated with the stripes of elevated strain that stretched across many channels that do not feature the ships signal (red, dashed line in Figure 1a, b). The strips were also detected in data recorded at 10:36:14 UTC on 2 November and at 02:00:02 UTC on 4 November, where also no ship was present (not shown).

We expect that some of those signals are related to ambient oceanic noise such as wave,[16] tidal,[25] seismic,[12,15,26–28] and biological sources[6,11,29] that dominates below 20 Hz or above 200 Hz.

However, Zak (2008)[2] associated a similar frequency of 8 Hz to the propeller shafts of Polish Navy ships as recorded simultaneously by both a hydrophone deployed in the water and by an accelerometer deployed close to the shafts. We can neither verify nor assess this statement in our study but require further examples of ship signals as well as details of their mechanical parts.

Our result is supported by Wilcock et al. (2023)[6] and Paap et al. (2025)[19] which used the same dataset. Wilcock et al. (2023)[6] associated elevated energy which they found in power spectral density and in spectrograms at frequencies between 10 Hz and 60 Hz to the passing ship. Paap et al. (2025)[19] found vessel-related energy at frequencies above 50 Hz and below 100 Hz in power spectral density. They argued that a frequency peak of 100 Hz is possibly induced by the alternating current inside of the power cable

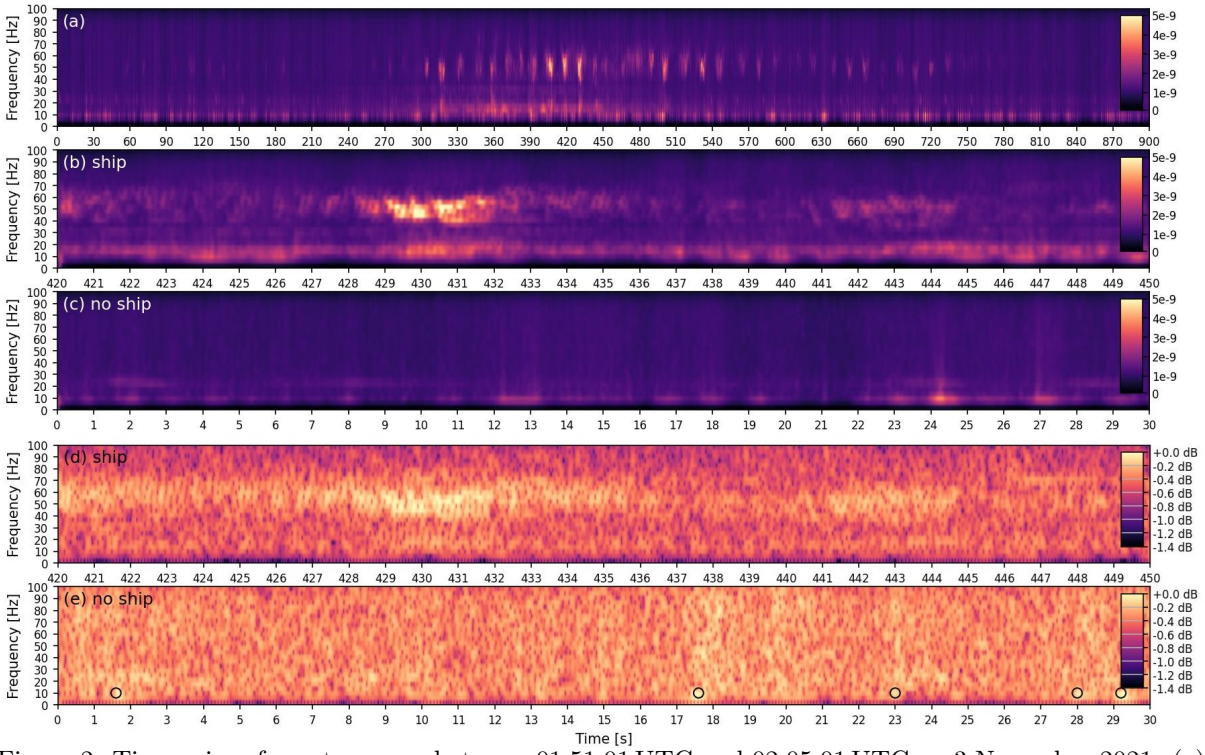

Figure 2: Timeseries of spectrograms between 01:51:01 UTC and 02:05:01 UTC on 3 November 2021. (a) Mean of all channels with #1670 channels from 23 000 to 24 470 between 46 900 m and 50 370 m distance from the coast. Each spectrogram segment is 30 s long. (b) Zoom-in, mean of all channels close to the ship's presence between 420 s and 450 s with start time 01:58:01 UTC (Figure 1b). (c) Zoom-in, mean of all channels between 0 s and 30 s with start time 01:51:01 UTC, no-ship case (Figure 1a). (d) Individual channel #23 960, ship's presence between 420 s and 450 s. (e) Individual channel #23 960, no-ship case between 0 s and 30 s.

they investigated. Other studies found energy emitted by ships at slightly different frequencies, though comparable, especially as different ships[3,19] with different machinery[2] traveling at different speeds[2] and at different distances to the cable were investigated. Besides different vessels and their propagation mode, the quality of the recordings is dependent on the cable coupling to the seafloor[13] and on the cable sensitivity related to its internal structure. Further, we expect that the bathymetry, the water column thickness between ship and cable as well as the water properties such as salinity that determines the density which in turn influences the sound speed cause variety in the acoustic signatures. Our finding is also supported by Rivet et al. (2021)[5] who stated a dominating frequency of 49 Hz related to a ship found by applying DAS to a cable off the coast of Toulon (France) deployed through steep bathymetry. Niu et al. (2017)[3] showed that the shipping noise of three different cargo ships traveling with different speeds in the Santa Barbara Channel (CA, USA) measured by hydrophones is strongest between 30 Hz and 100 Hz which also supports the frequency range 40 to 65 Hz.

3.3 Energy envelope and spectral entropy

The energy envelope of an oscillating signal is a curve outlining its extreme. Here, we used it to assess whether the energy represented in the oscillating strain is significant and, thus, can be used to detect the

ship. We calculated the energy envelope as the discrete, linear convolution of the channel-wise squared strain and the inverse of 30% of the sampling frequency. We used a threshold of two standard deviations from the mean of the energy envelope to assess whether a signal from a ship was detected.
Averaging the energy envelope over all channels, as we have done for the spectrograms (Figure 2), eroded the ship's signal (not shown) and no significant information could be retrieved. Thus, we investigated the performance of detecting the ship using the energy envelope for the individual channel #23 960. The energy envelope during the ship's presence significantly increased above its mean value between 429 s and 432 s (red dots in Figure 3a), when the amplitudes of the spectrograms were also highest (Figure 2b, d). For the remaining time of the 30 s timeseries, the energy envelope was close to its mean value (blue, dashed line). We chose the two standard deviation as a detection threshold for the ship (blue, shaded area). Every value that exceeded two times the standard deviation around the mean, indicated a statistically significant deviation from the ambient noise. Thus, this was an event with significantly more energy than the ambient noise and, here, associated with energy emitted by the passing ship.

For the no-ship case (Figure 3b), the mean energy envelope was on average a magnitude of order

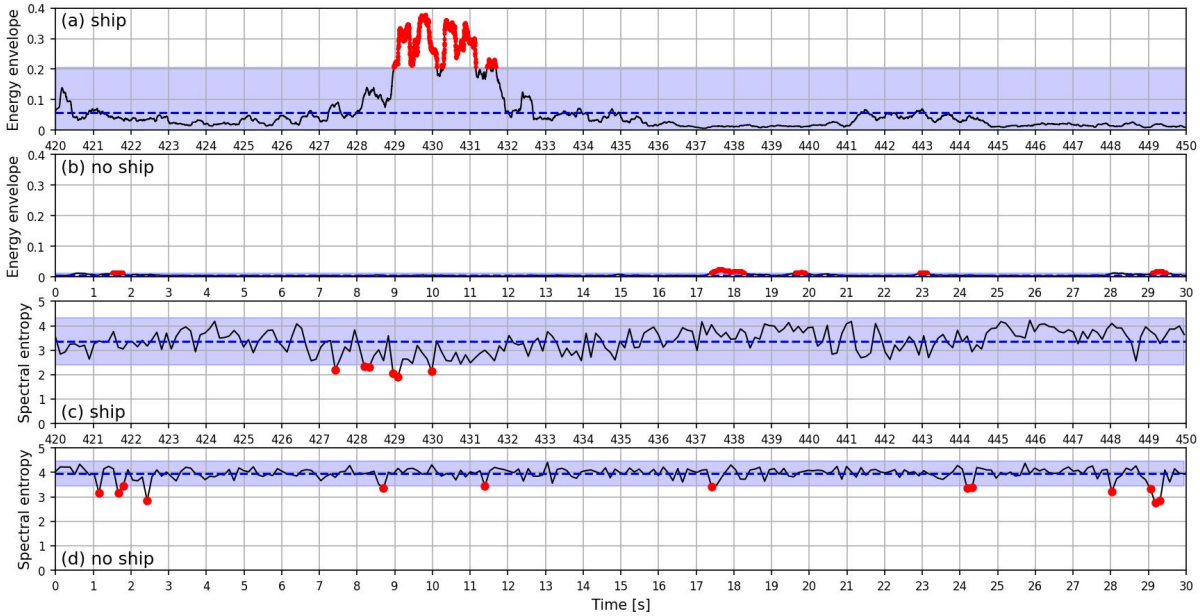

Figure 3: Timeseries of the energy envelope and the spectral entropy for the channel #23 960 and with a window size of 30 s on 3 November 2021. Energy envelope $[nstrain^2\ s]$ and spectral entropy for the ship (a, c) and the no-ship case (b, d), respectively. The blue dashed lines indicate the respective mean values and the blue shaded areas two standard deviations around the mean value.

lower than the energy envelope associated with the ship's presence (Figure 3a). During five events in the timeseries, the energy envelope also exceeded values of two standard deviations above its mean. However, the energy of those events were centered at frequencies of 10 Hz as shown in the respective spectrogram (Figure 3e).

The entropy is a measure that quantifies the disorder of a system. A high entropy is attributed to ambient noise, here, the ocean state when it is undisturbed by the ship. The spectral entropy is a measure of the spectral energy distribution of a signal which quantifies the peakiness of its frequency content. Hereby, the normalized energy spectrum is treated as a probability distribution. A higher spectral entropy indicates a more even distribution of energy across frequencies while a lower entropy suggests a

more concentrated or peaky spectrum. Thus, a decrease in entropy suggests an event occurring that is different from the ambient noise.
We have computed the spectral entropy in three steps. Firstly, we computed the absolute square of the STFT of the strain. Secondly, we normalized the absolute square of the STFT by its sum, referred to as ratio. Lastly, we defined the spectral entropy as the negative sum of the product of the ratio and the base-2 logarithmic of the ratio. We used a threshold of two standard deviations from the mean of the spectral entropy to assess whether a signal from a ship is detected.
The spectral entropy during the ship's presence significantly decreased below the two standard deviation threshold from its mean between 427 s and 430 s (red dots in Figure 3c). Thus, this time period indicate an event with significantly less entropy than the ambient noise and is associated with the ship. The time period partly overlapped with when the dB-scaled spectrograms and the energy envelope were highest (Figures 2d and 3a), however, the spectral entropy decreased shortly before. For the remaining time, the spectral entropy oscillated around its mean value (blue, dashed line, Figure 3c).
The mean of the spectral entropy for the ship's presence was lower than of the ocean state without the ship's presence (Figure 3c, d). This strengthens the assumption that the signal originated from the passing ship and is not associated with the background noise of the ocean.

The energy envelope and the spectral entropy are useful in detecting ships when individual channels of the cable are considered. Further, Rivet et al. (2021)[5] discusses that spectral features at different frequency of the same ship might not always be present, depending on changes in the ship's speed, the heterogeneous coupling of the cable to the ground, and the greater attenuation of the acoustic waves with water column depth. This might explain, why the ship's signal can only be robustly detected based on our detection threshold of two standard deviations during a short time period when it is strong enough, here, between 9 s and 12 s and between 7.5 s and 10 s. Possibly, the interaction of the signal from a specific part at a specific frequency might interact with another part of the ship, e.g., its hull, which might alter the frequency.

3.4 Frequency index

The frequency index (FI) quantifies the occurrence of a particular event that is prominent against noise. Here, we used the FI to assess whether the presence of acoustics signals emitted by the ship overlaying the ambient noise of the ocean is significant. We calculated the FI for the selected channels (#1670) of the ship and the no-ship cases as such that one FI represents one channel. We filtered the amplitudes of the spectrograms based on defined lower and upper frequency bands each consisting of two frequencies that represent and also constrain the ambient noise (lower) and the event/ship (upper). Subsequently, we computed the FI as the base-10 logarithmic of the ratio of the mean amplitude of the spectrogram within the upper frequency band and the mean amplitude within the lower frequency band. The FI for each individual channel represent one value of a distribution.
Figure 4 shows the FI distributions for the no-ship case (a) and the ship case (b). The distribution for the no-ship case (a) is characterized by a long tail of negative FI and has a width of 0.76. In contrast, the FI distribution for the ship case (b) is with 1.43 significantly broader. This results from the significantly more pronounced tail towards positive FI which is the characteristic behavior that differentiates it from a normal and from the no-ship distributions. Thus, we conclude that the long tail of positive FI is a robust detector for the ship's presence.

The FI distribution for the ship case is closer to a normal distribution with more distributed data. More distributed data indicate an event that creates variations such as the presence of a ship. Thus, the distribution represents more consistent activity rather than sporadic events with lower noise, which we expect from ship signatures compared to ambient noise. In both cases, there is a relatively balanced contribution between the upper and lower frequency bands, which yields values between 0 and 0.2 due

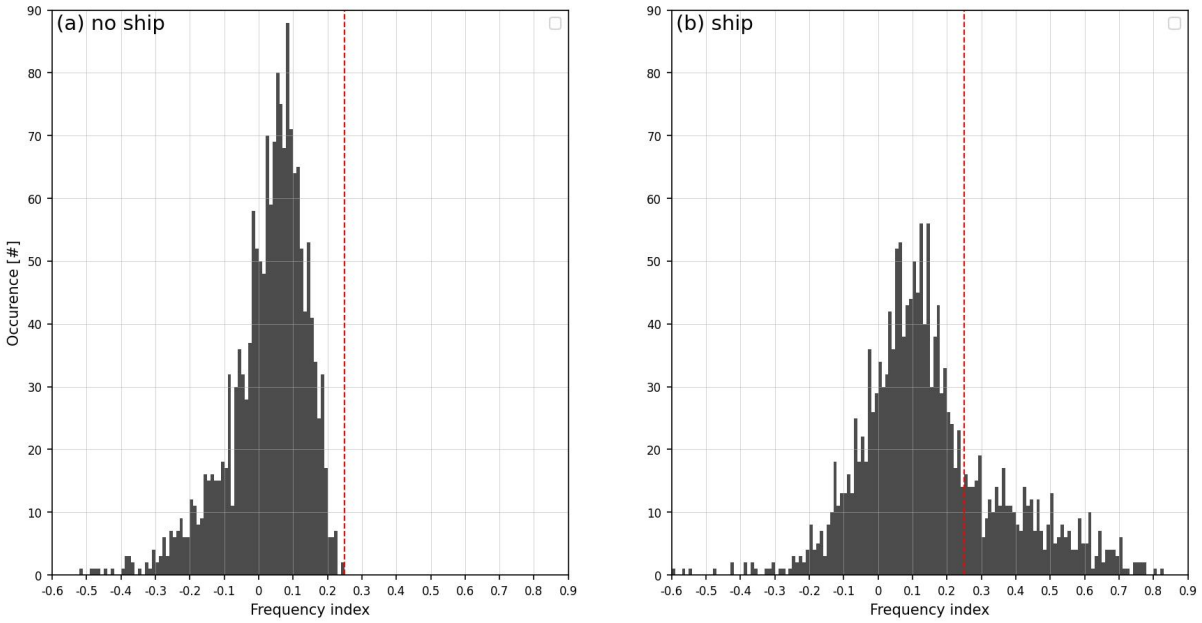

Figure 4: Distribution of the frequency index (FI) with a bin width of 0.01 as computed from spectrograms for the no-ship (a) and ship (b) cases. Lower and upper frequency bands are 0-10 Hz and 45-55 Hz, respectively. The red, dashed lines represent the maximum FI of the no-ship distribution in (a).

to oceanic noise. Hence, the no-ship case yields a signal whose FI present a narrow, peaked distribution, whereas when the ship is present, the distribution flattens and broadens. These results confirm the importance of careful upper frequency selection for ship detection, suggesting that the lower band is adequately selected at 0–10 Hz.

4. CONCLUSION AND OUTLOOK

We identified the signal processing parameters energy envelope, spectral entropy, and frequency index based on strain data to be useful in detecting a ship that passed a pre-installed underwater telecommunication cable using DAS. Those parameters complement the signal processing tools of 1) spectrograms and 2) power spectral density, which has been demonstrated to detect ships in previous studies. Hence, we suggest to take into account those parameters for ship detection using DAS in developing automated detection algorithms and classification schemes. The frequencies at which ships emit acoustic energy are thereby essential to successfully use those tools. We found the maximum energy emitted from a ship and received at a cable at frequencies between 40 Hz and 60 Hz. In this study, the distribution of the frequency index for the presence of a ship was characterized by a long tail towards positive values. We showed that the energy envelope and the spectral entropy deviated significantly from their mean as a response to the presence of the ship.

To validate and expand the use of those parameters for robust ship detection, the existing DAS databases of vessel signatures, e.g. PubDAS[30] need expanded. Thereby, dependencies of the data on the environmental conditions (ambient noise, bathymetry, salinity, water column thickness between vessel and fiber), ship characteristics (size, geometry, speed, machinery, distance and angle to fiber), cable types and properties as well as measuring parameters (sampling frequency, gauge length, channel spacing), and measuring methods which depend on the interrogators need to be considered and disentangled. This includes also the acoustic signatures of smaller objects such as AUVs,[31] ROVs,[32] small boats,[4] anchor drops, and even

human divers that might be retrievable with DAS. To develop such a database, DAS interrogators need to be connected to many more underwater power and telecommunication cables to record relevant data. This requires further communication with authorities, stakeholders, and cable providers, on a national as well as an international basis. Such a database would serve as the base in algorithm development for real-time data analyses, pattern detection and recognition, classification, and perimeter control to advance in protecting our maritime cable infrastructure.

ACKNOWLEDGMENTS

The study was funded by the German Aerospace Center (DLR e. V.). We thank T. Flenker (DLR e. V.) for providing the AIS tool and for his instructions to use it.

REFERENCES

[1] Hartog, A. H. *An Introduction to Distributed Optical Fibre Sensors* (CRC Press, Boca Raton, FL, USA, 2017), 1st edn.

[2] Zak, A. Ships classification basing on acoustic signatures. *WSEAS Transactions on Signal Processing* **4**, https://www.scopus.com/inward/record.uri?eid=2-s2.0-48849115518&partnerID=40&md5=e3376bb558615a0503df876641329e26 (2008).

[3] Niu, H., Ozanich, E. & Gerstoft, P. Ship localization in santa barbara channel using machine learning classifiers. *The Journal of the Acoustical Society of America* **142**, https://doi.org/10.1121/1.5010064 (2017).

[4] Reis, C. D. G., Padovese, L. R. & de Oliveira, M. C. F. Automatic detection of vessel signatures in audio recordings with spectral amplitude variation signature. *Methods in Ecology and Evolution* **10**, https://doi.org/0.1111/2041-210X.13245 (2019).

[5] Rivet, D., de Cacqueray, B., Sladen, A., Roques, A. & Calbris, G. Preliminary assessment of ship detection and trajectory evaluation using distributed acoustic sensing on an optical fiber telecom cable. *The Journal of the Acoustical Society of America* **149**, https://doi.org/10.1121/10.0004129 (2021).

[6] Wilcock, W. S. D., Abadi, S. & Lipovsky, B. P. Distributed acoustic sensing recordings of low-frequency whale calls and ship noise offshore central oregon. *JASA Express Letters* **3**, https://doi.org/10.1121/10.0017104 (2023).

[7] Bueno Rodriguez, A. *et al.* DASBoot: an annotation toolkit for DAS-based maritime surveillance. In Bouma, H., Prabhu, R., Yitzhaky, Y. & Kuijf, H. J. (eds.) *Artificial Intelligence for Security and Defence Applications II*, vol. 13206, https://doi.org/10.1117/12.3031529. International Society for Optics and Photonics (SPIE, 2024).

[8] Gurevich, B. *et al.* Detection of aircraft noise using distributed acoustic sensing with a buried telecommunication cable. *NPJ Acoustics* **1**, https://doi.org/10.1038/s44384-025-00007-8 (2025).

[9] He, Z. *et al.* Fiber-optic distributed acoustic sensors (das) and applications in railway perimeter security. In Liu, T. & Jiang, S. (eds.) *Advanced Sensor Systems and Applications VIII*, vol. 10821, https://doi.org/10.1117/12.2505342 (SPIE, 2018).

[10] Bouffaut, L. *et al.* Eavesdropping at the speed of light: Distributed acoustic sensing of baleen whales in the arctic. *Frontiers in Marine Science* **9**, https://doi.org/10.3389/fmars.2022.901348 (2022).

[11] Landrø, M. *et al.* Sensing whales, storms, ships and earthquakes using an arctic fibre optic cable. *Scientific Reports* **12**, https://doi.org/10.1038/s41598-022-23606-x (2022).

[12] Fernández-Ruiz, M. R. *et al.* Seismic monitoring with distributed acoustic sensing from the near-surface to the deep oceans. *Journal of Lightwave Technology* **40**, https://doi.org/10.1109/JLT.2021.3128138 (2022).

[13] Lior, I. *et al.* On the detection capabilities of underwater distributed acoustic sensing. *Journal of Geophysical Research Solid Earth* **126**, https://doi.org/10.1029/2020JB020925 (2021).

[14] Lindsey, N. J., Dawe, T. C. & Ajo-Franklin, J. B. Illuminating seafloor faults and ocean dynamics with dark fiber distributed acoustic sensing. *Science* **366**, https://doi.org/10.1126/science.aay5881 (2019).

[15] Williams, E. F. *et al.* Distributed sensing of microseisms and teleseisms with submarine dark fibers. *Nature Communications* **10**, https://doi.org/10.1038/s41467-019-13262-7 (2019).

[16] Smith, M. M., Thomson, J., Baker, M. G., Abbott, R. E. & Davis, J. Observations of ocean surface wave attenuation in sea ice using seafloor cables. *Geophysical Research Letters* **50**, https://doi.org/10.1029/2023gl105243 (2023).

[17] Baker, M. G. & Abbott, E. Rapid refreezing of a marginal ice zone across a seafloor distributed acoustic sensor. *Geophysical Research Letters* **44**, https://doi.org/10.1029/2022GL099880 (2022).

[18] Ugalde, A. *et al.* Noise levels and signals observed on submarine fibers in the canary islands using das. *Seismological Research Letters* **93**, https://doi.org/10.1785/0220210049 (2022).

[19] Paap, B., Vandeweijer, V., van Wees, J.-D. & Kraaijpoel, D. Leveraging distributed acoustic sensing for monitoring vessels using submarine fiber-optic cables. *Applied Ocean Research* **154**, https://doi.org/10.1016/j.apor.2025.104422 (2025).

[20] SEAFOM, Fiber, Optic, Monitoring & Group. Document no: Seafom measuring sensor performance document – (seafom msp-02 v2.0) das parameter definitions and tests. Tech. Rep. (2024).

[21] Ip, E. *et al.* Using global existing fiber networks for environmental sensing. *IEEE* **110**, https://doi.org/10.1109/JPROC.2022.3199742 (2022).

[22] Wilcock, W. S. D., Ocean, Observatories & Initiative. Rapid: A community test of distributed acoustic sensing on the ocean observatories initiative regional cabled array [dataset], https://doi.org/10.58046/5J60-FJ89 (2023).

[23] Sifakis, N. & Tsoutsos, T. Shipping: Setting sail - challenges for sea transport. *Heinrich Böll Stiftung, Access 2025-07-30,* https://eu.boell.org/en/shipping-setting-sail-challenges-for-sea-transport (2021).

[24] Flenker, T. & Stoppe, J. Marlin: An iot sensor network for improving maritime situational awareness. In *MARESEC 2021* (MARESEC, Bremerhaven, Germany, 2021).

[25] Becker, M. W. & Coleman, T. I. Distributed acoustic sensing of strain at earth tide frequencies. *Sensors* **19**, https://doi.org/10.3390/s19091975 (2019).

[26] Lindsey, N. J., Rademacher, H. & Ajo-Franklin, J. B. On the broadband instrument response of fiber-optic das arrays. *Journal of Geophysical Research: Solid Earth* **125**, https://doi.org/10.1029/2019JB018145 (2020).

[27] Baird, A. F. *et al.* Characteristics of microseismic data recorded by distributed acoustic sensing systems in anisotropic media. *Geophysics* **85**, https://doi.org/10.1190/geo2019-0776.1 (2020).

[28] Lellouch, A., Lindsey, N. J., Ellsworth, W. L. & Biondi, B. L. Comparison between distributed acoustic sensing and geophones: Downhole microseismic monitoring of the forge geothermal experiment. *Seismological Research Letters* **91**, https://doi.org/10.1785/0220200149 (2020).

[29] Mellinger, D. K. & Clark, C. W. Blue whale (balaenoptera musculus) sounds from the north atlantic. *Acoust Soc Am* **114**, https://doi.org/10.1121/1.1593066 (2003).

[30] Spica, Z. J. *et al.* Pubdas: A public distributed acoustic sensing datasets repository for geosciences. *Seismological Research Letters* **94**, https://doi.org/10.1785/0220220279 (2023).

[31] Millard, N. W. *et al.* Versatile autonomous submersibles—the realising and testing of a practical vehicle. *Underwater Technology* **23**, https://doi.org/10.3723/175605498783259894 (1998).

[32] Anhaus, P. *et al.* Under-ice environment observations from a remotely operated vehicle during the mosaic expedition. *Scientific Data* **12**, https://doi.org/10.1038/s41597-025-05223-1 (2025).